Appendix

A.1 Working with Electrical Aircraft Machines

A.1.1 Original Master Thesis Agreement

NTNU and Rolls-Royce are working on sustainable technologies for the future ”more electric aircraft” (MEA). Preliminary work on the thermal management and engine cooling system concepts has been done for a high-efficient electrical machine. Further studies will focus on completing the design and physical testing of an experimental motor.

1. The machine designed in the project work shall be completed and tested. This involves completion of the physical machine design, design of the ancillary cooling circuit, and necessary instrumentation. Also, a test program shall be made and executed in cooperation with the other students involved. An uncertainty analysis of the thermal behavior shall be carried out. The results shall be presented, analyzed, discussed and compared to analysis. Where relevant, additional modeling for improving the thermal predictions shall be made. Based on the results, suggestions for improving the machine design shall be discussed.

The heating caused by electrical resistance within the conducting wires of electrical engines can become critical in high current density machines. In order to create better thermal models, a study will be performed regarding the effective transverse and longitudinal thermal conductivity of the windings.

2. A calculation model shall be established for the calculation of transverse and longitudinal temperature distribution in electrical wire mesh conductors having internal heat generation due to ohmic resistance. Wire mesh geometries and resin materials shall be defined in cooperation with the Department. Relevant factors influencing the heat flow and temperature distribution shall be investigated. Based on model calculations, simplified ‘engineering’-type correlations/models shall be proposed.
3. Suggestions for further work shall be presented and discussed.

A.1.2 Some Experiences from the Project

This project has been a collaboration between different engineering fields at the Norwegian university of science and technology (NTNU) and Rolls Royce, a commercial company. The goal was to design and build a compact machine prototype for testing, providing valuable experience for the development of electrical motors for aircraft applications.

As of this report, no actual prototype has been built, and the initial focus of this thesis has been changed. This is partly due to the outbreak of COVID-19, but also because the design process took longer time than expected. For the future work with this machine, as well as the development of electrical machines in general, a few notes on the project and practical experiences have been written down in this section.

Working on this machine required the collaboration between thermal, electrical and mechanical engineers, as well as a cooperation between the university and the company. As has been mentioned multiple times in the report, a good integration of the different engineering aspects are needed when working with such projects, since many of the design choices and options for optimization intertwine with each other. However, during the work, more focus was given to the isolated, individual aspects than how they worked together in the final product. Of course, less focus was needed on the prototype after it was found that it would not be built, but this issue was present from the beginning. In this initial phase, focusing on the separate phenomena, presenting more in-depth analysis may be an advantage, and so the segregation of the theses could be justified.

As a consequence, before the construction plans were abandoned, a lot of time was given to the union of the three separate evaluations in order to construct a feasible product. Included in this work was also acquisition of the necessary parts lists and quotations for the manufacturing and assembly. At some point, more time was given to organization and planning than to the research itself. Since most of the job on developing the plans for the prototype as well as the acquisition of the necessary parts were our, the students' responsibility, the split focus slowed down progress. This affected both the ordering process as well as the studies themselves. Already before campus locked down due to the virus there were concerns that the building of the machine would not be able to be finished in time.

When working with such a multidisciplinary project involving multiple members from both academic and commercial backgrounds, it is important to establish good structures for cooperation in order to use as much as possible of each participant's expertise. In future work, this could be achieved by:

A. Establishing proper agreements between the parties, clarifying responsibilities and setting the organizational structure

B. Establishing a leader responsible for mapping out the project's goals and checking up on progress (this can be from the company, the university or both)

C. Encouraging the multidisciplinary cooperation by combining the individual work into one thesis, or by simply locating the participants' offices closer to one another

A.1.3 Some of the More Important Sources

The following list is a collection of the literature considered most important for this work:

- Basic concepts:

  Hanselman 2006, *Brushless Permanent Magnet Motor Design*

  Incropera et al. 2013, *Principles of Heat and Mass Transfer*

- Electric aircraft machines:

  Christie, Dubois, and Derlaga 2017, *Cooling of Electric Motors Used for Propulsion on SCEPTOR*

  Duffy et al. 2018, "Propulsion Scaling Methods in the Era of Electric Flight"

  Hepperle 2012, "Electric Flight - Potential and Limitations"

  Yi and Haran 2019, "Thermal Integration of a High-Frequency High-Specific-Power Motor within Electrically Variable Engine"

  Zhang et al. 2018, "Large electric machines for aircraft electric propulsion"

- Thermal management of electrical motors:

  Huang et al. 2012, "Direct Oil Cooling of Traction Motors in Hybrid Drives"

  Tüysüz et al. 2017, "Advanced Cooling Methods for High-Speed Electrical Machines"

  Yang et al. 2016, "Thermal Management of Electric Machines"

  Yi 2016, "Electromagnetic-thermal modeling for high-frequency air-core permanent magnet motor of aircraft application"

- Air gap heat transfer:

  Fénot et al. 2011, "A Review of Heat Transfer Between Concentric Rotating Cylinders with or without Axial Flow"

- Winding homogenization:

  Ayat et al. 2018, "Estimation of Equivalent Thermal Conductivity for Electrical Windings with High Conductor Fill Factor"

  Jaritz and Biela 2013, "Analytical model for the thermal resistance of windings consisting of solid or litz wire"

  Liu et al. 2019, "Comparative study of thermal properties of electrical windings impregnated with alternative varnish materials"

  Wrobel, Ayat, and Baker 2017, "Analytical methods for estimating equivalent thermal conductivity in impregnated electrical windings formed using Litz wire"

  Yi et al. 2019, "Equivalent Thermal Conductivity Prediction of Form-Wound Windings with Litz Wire Considering Transposition Effect"

A.2 FE Temperature Fields from First Iteration

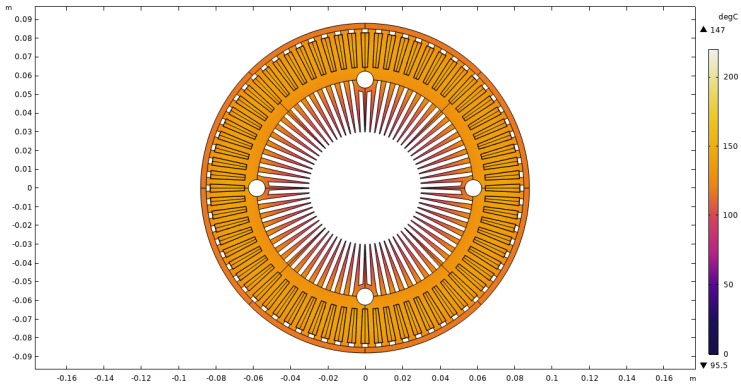

(a) Inlet/outlet section, T_b at inlet temperature and outlet temperature.

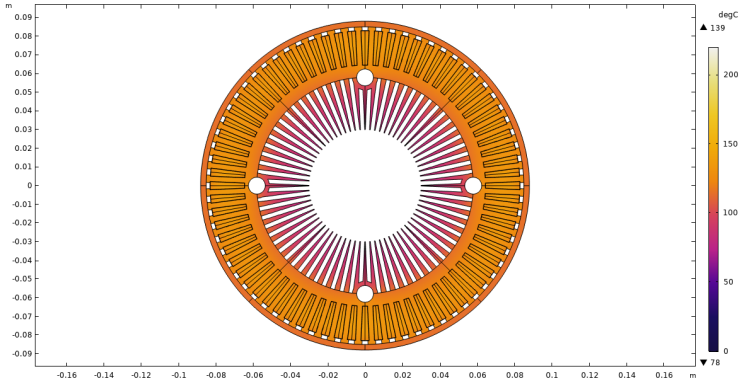

Middle section.

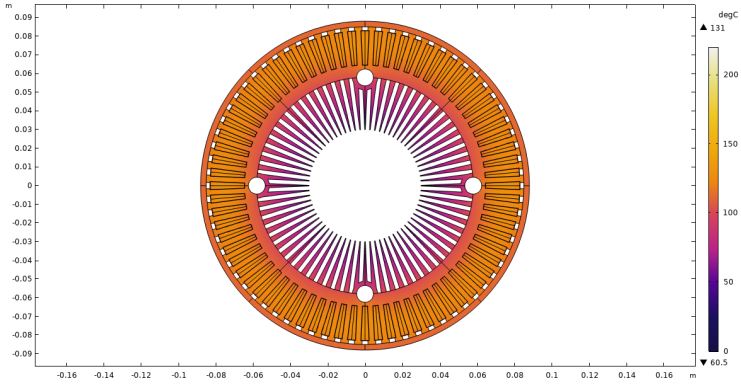

End section, T_b equal on both sides.

Figure A.1: FEM analysis using axial evolution of h and T_b. 72 fins.

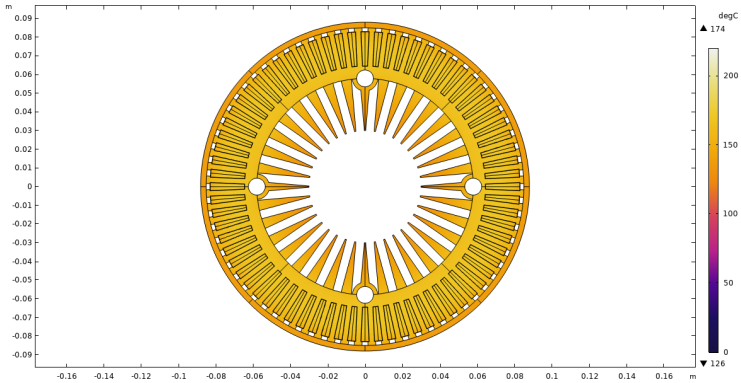

(a) Inlet/outlet section, T_b at inlet temperature and outlet temperature.

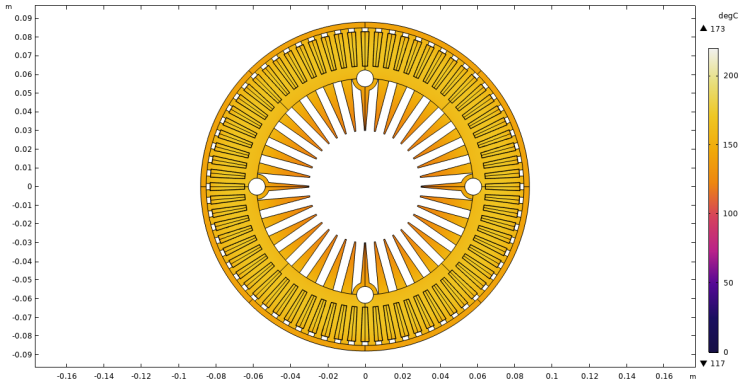

(b) Middle section.

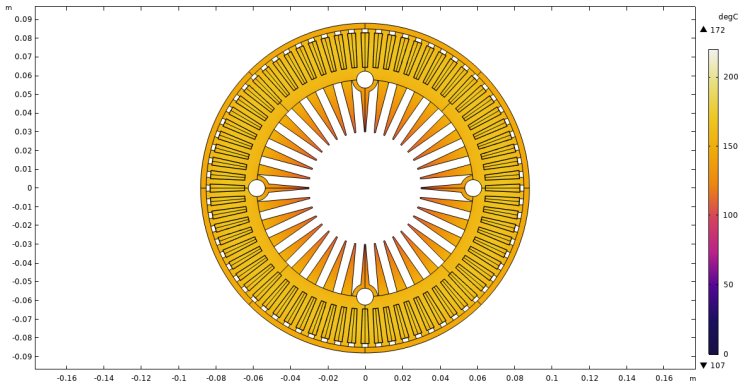

(c) End section, T_b equal on both sides.

Figure A.2: FEM analysis using axial evolution of h and T_b. 36 fins.

A.3 Stator Geometry

[Confidential]

A.4 MIDEL 7131 Thermal Properties

Midel 7131 Thermal Properties					
Temperature [°C]	Kinematic Viscosity [mm^2/s]	Density [kg/m^3]	Specific Heat Capacity [J/kg/K]	Thermal Conductivity [W/m/K]	Thermal Expansion Coefficient [1/K]
-30	4200	1007	1783,00	0.1451	0.00072
-20	1400	1000	1797	0.1453	0.00073
-10	430	992	1811	0.1452	0.00074
0	240	985	1830	0.1451	0.00074
10	125	978	1855	0.1448	0.00075
20	70	970	1880	0.1444	0.00075
30	43	963	1910	0.1438	0.00076
40	28	956	1933	0.1430	0.00077
50	19.5	948	1959	0.1422	0.00077
60	14	941	1994	0.1412	0.00078
70	10.5	934	2006	0.1400	0.00078
80	8	926	2023	0.1387	0.00079
90	6.5	919	2040	0.1372	0.00079
100	5.25	912	2058	0.1357	0.00080
110	4.4	904	2075	0.1339	0.00082
120	3.7	897	2090	0.1320	0.00082
130	3.2	890	2116	0.1300	0.00083
140	2.8	882	2145	0.1279	0.00084

Source
http://www.midel.com/productsmidel/midel-7131/thermal-properties

MIDEL 2018.

A.5 COM-Model $\dot{m}$-Analysis

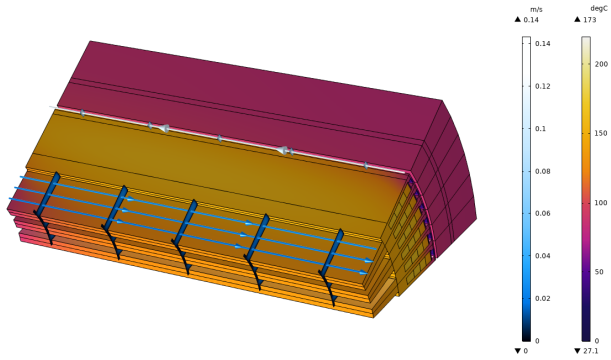

(a) COM-model temperature field and oil channel flow analysis. $\dot{m} = 0.035kg/s$.

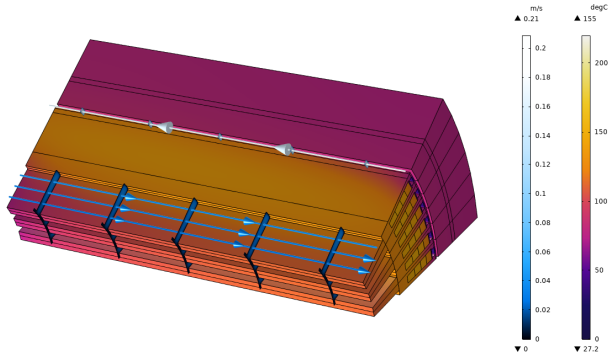

(b) COM-model temperature field and oil channel flow analysis. $\dot{m} = 0.05kg/s$.

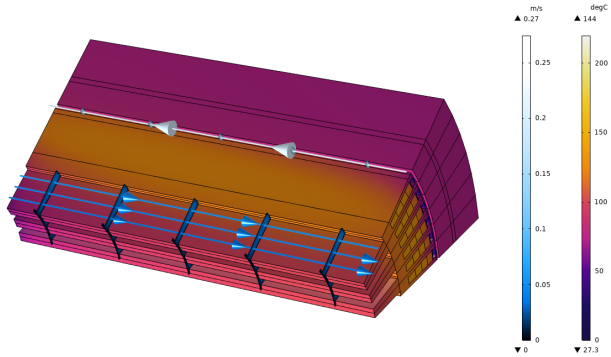

(c) COM-model temperature field and oil channel flow analysis. $\dot{m} = 0.065kg/s$.

Figure A.3: Comparison of the COM-model run for three different oil mass flow rates.

A.6 COM Sensitivity Analysis

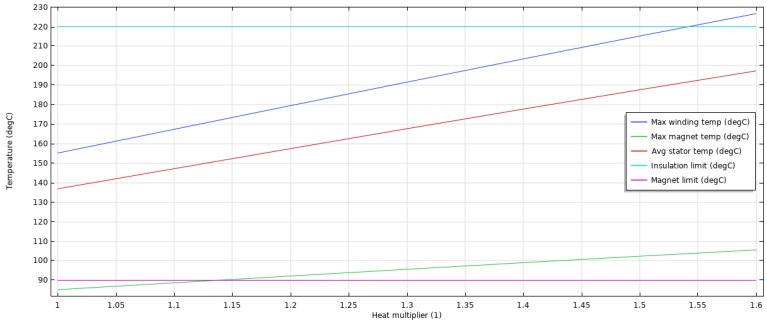

(a) $\dot{Q}_S$ temperature sensitivity.

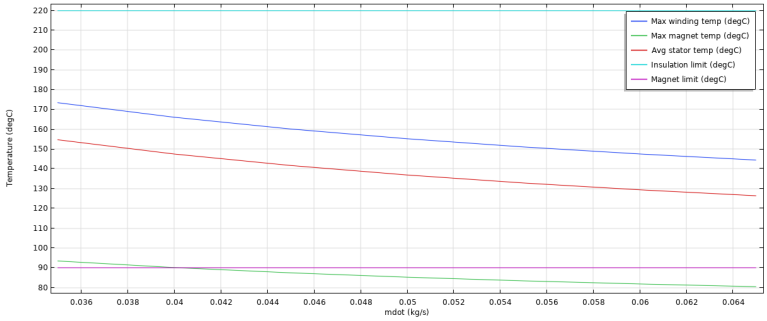

(b) $\dot{m}$ temperature sensitivity.

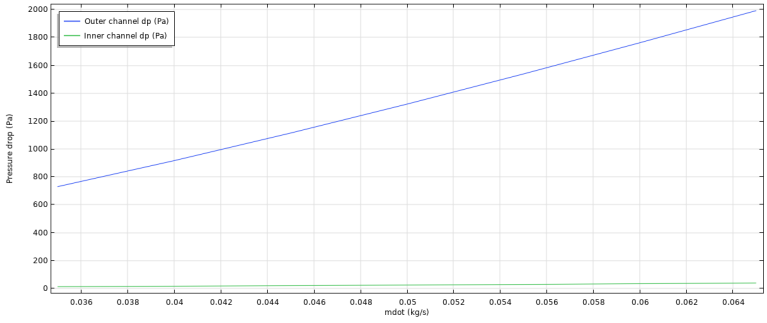

(c) $\dot{m}$ pressure sensitivity.

Figure A.4: Sensitivity analysis.

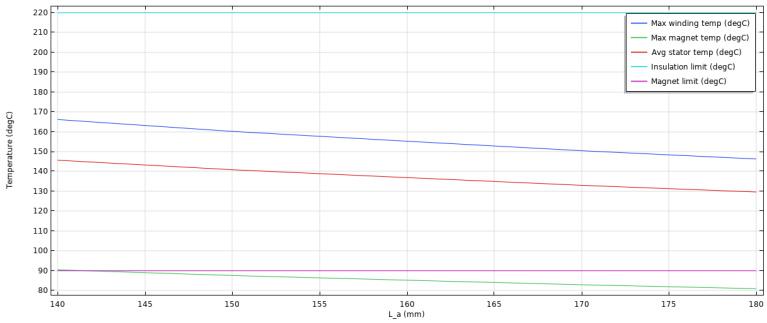

(d) L_A temperature sensitivity.

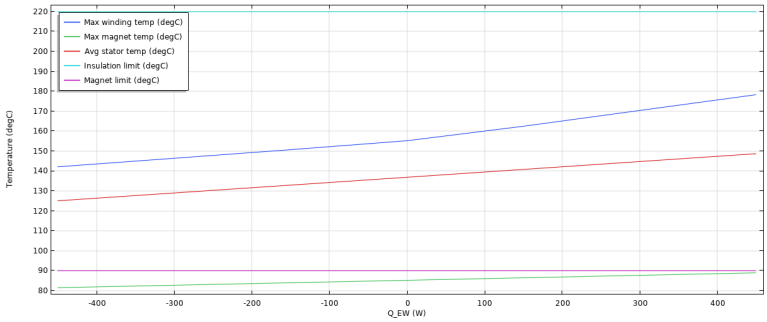

(e) $\dot{Q}_{EW}$ temperature sensitivity.

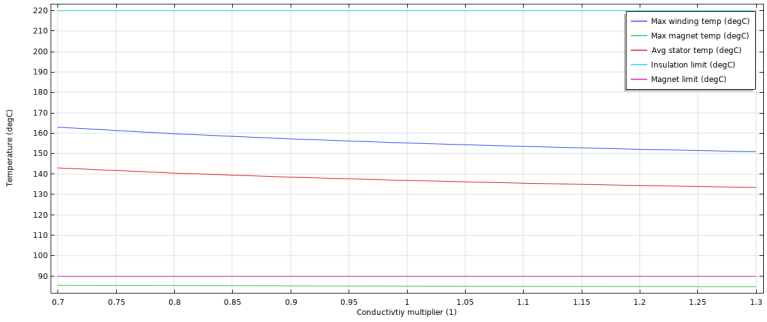

(f) k_L temperature sensitivity.

Figure A.4: Sensitivity analysis (cont.).

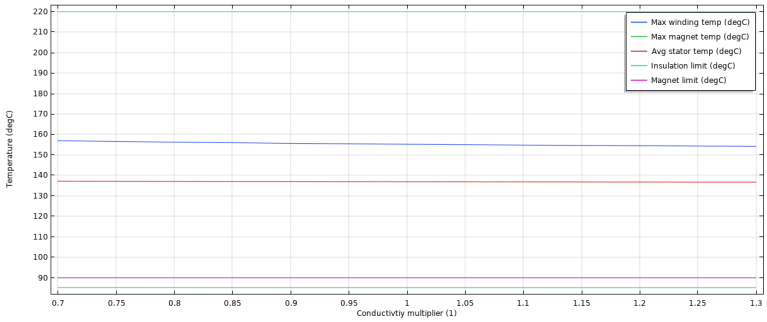

(g) k_W temperature sensitivity.

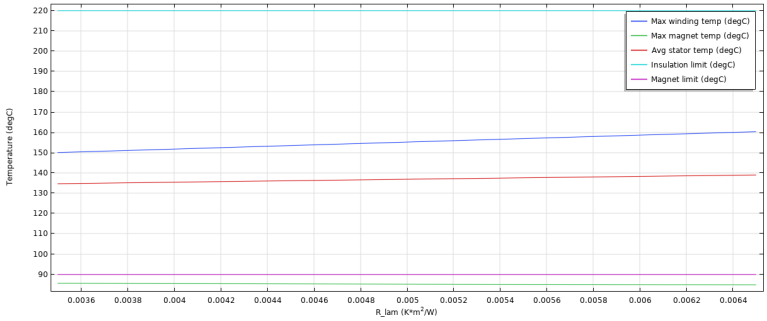

(h) $\mathbb{R}''_W$ temperature sensitivity.

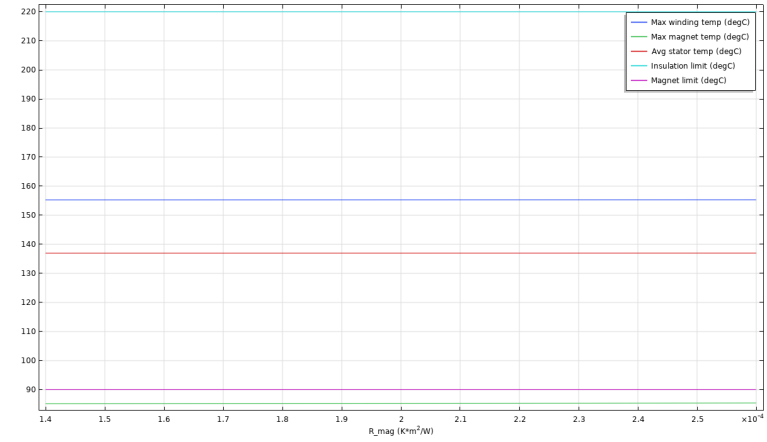

(i) $\mathbb{R}''_R$ temperature sensitivity.

Figure A.4: Sensitivity analysis (cont.).

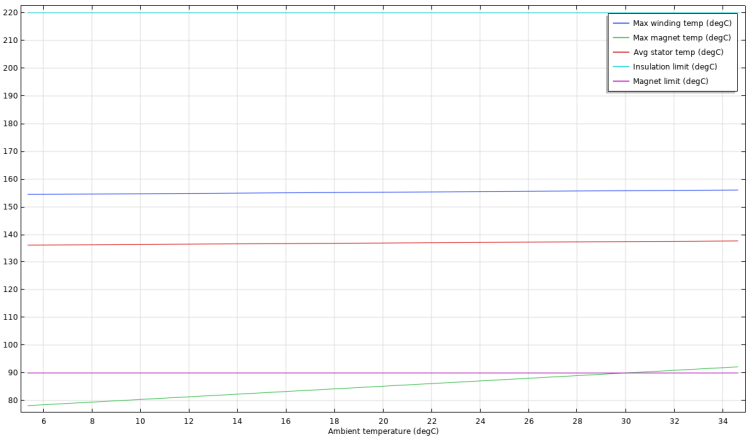

(j) T_{amb} temperature sensitivity.

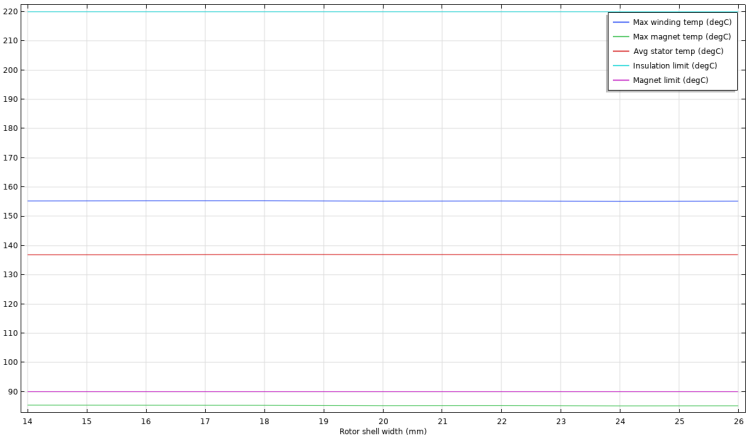

(k) t_R temperature sensitivity.

Figure A.4: Sensitivity analysis (cont.).

A.7 Air Gap Windage Loss Correlations

A.7.1 Experimental data (1970 report)

An experiment was carried out by Gorland, Kempke, and Lumannick in 1970 studying the windage loss in the air gap between two concentric cylinders with the innermost rotating at specific rotational speeds. Three air gap widths were tested: 0.0565in (1.44mm), 0.116in (2.95mm), and 0.236in (6.00mm). A relation was found between the friction factor, λ, the air gap width and the rotational speed. Some of the tabulated values from this report are shown in the graph in figure A.5, in which the linearly interpolated values for a 2mm air gap are imposed.

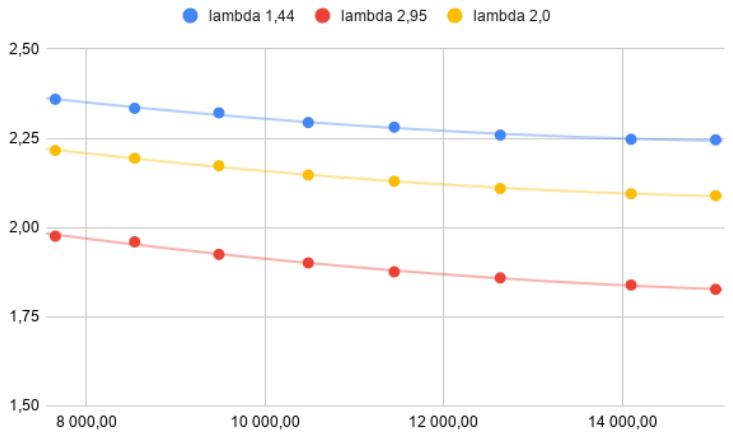

Figure A.5: Friction factor λ for set air gap sizes [1.44mm, 2.00mm, 2.95mm].

A.7.2 Correlation equations

Zheng et al. 2005:

$$C_w = 0.0095 \left(\sqrt{Ta}\right)^{-0.2} \tag{A.1}$$

Gao and Yu 2013:

$$C_w = \frac{0.0152\kappa}{Re_{\theta,ag}^{0.24}} \left[1 + \left(\frac{7Re_{z,ag}}{2Re_{\theta,ag}}\right)^2\right]^{0.38} \tag{A.2}$$

$$\kappa = 1.3 \tag{A.3}$$

A.8 Air Gap Convection Correlations

Equations may be modified from the source to fit the current definition of Nu.

Kosterin and Finatev 1962

$$Nu_{ag} = 0.018\overline{Re}^{0.8} \tag{A.4}$$

$$\overline{Re} = \sqrt{Re_{z,ag}^2 + 0.6Re_{\theta,ag}^2} \tag{A.5}$$

Grosgeorge 1983

$$Nu_{ag} = 0.00368Re_{z,ag}^{0.175}Pr^{\frac{1}{3}}\overline{Re}^{0.8} \tag{A.6}$$

$$\overline{Re} = \sqrt{Re_{z,ag}^2 + 0.8Re_{\theta,ag}^2} \tag{A.7}$$

Bouafia et al. 1998

$$Nu_{ag,R} = 0.025\overline{Re}_1^{0.8} \tag{A.8}$$

$$\overline{Re}_1 = \sqrt{Re_{z,ag}^2 + 0.5Re_{\theta,ag}^2} \tag{A.9}$$

$$Nu_{ag,S} = 0.046\overline{Re}_1^{0.7} \tag{A.10}$$

$$\overline{Re}_1 = \sqrt{Re_{z,ag}^2 + 0.25Re_{\theta,ag}^2} \tag{A.11}$$

Poncet, Haddadi, and Viazzo 2011

$$Nu_{ag,R} = 0.0582Re_{\theta,ag}^{0.82}Pr^{0.3}\Phi^{0.09} \tag{A.12}$$

$$Nu_{ag,S} = 0.0908Re_{\theta,ag}^{0.75}Pr^{0.8}\Phi^{0.08} \tag{A.13}$$

$$\Phi \in [0, 3.0 \times 10^4]$$

	$\boldsymbol{\Gamma}$	$\boldsymbol{\varrho}$	$\boldsymbol{Re_{z,ag}}$	$\boldsymbol{Re_{\theta,ag}}$	$\boldsymbol{Ta}$
Kosterin and Finatev	77.5	0.78	$[3.1 \times 10^4, 3.0 \times 10^5]$	N/A	$[0, 8.0 \times 10^5]$
Grosgeorge	200	0.98	$[9.9 \times 10^3, 2.7 \times 10^4]$	N/A	$[1.4 \times 10^5, 4.9 \times 10^6]$
Bouafia et al.	98.4	0.956	$[1.1 \times 10^4, 3.1 \times 10^4]$	N/A	$[1.8 \times 10^3, 4.0 \times 10^6]$
Poncet, Haddadi, and Viazzo	76.9	0.961	Φ	$[3.7 \times 10^3, 3.7 \times 10^4]$	N/A

Table A.1: Nusselt correlation limits

A.9 Air gap CFD results

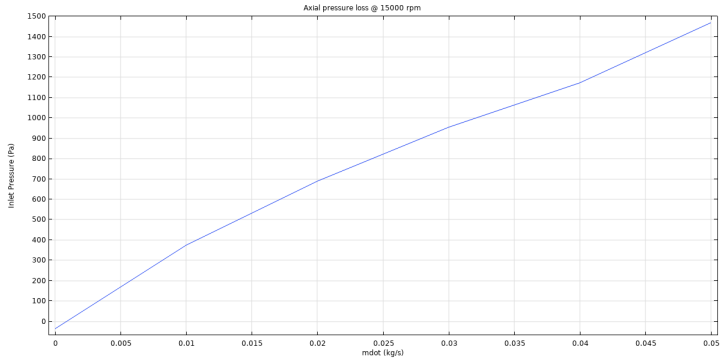

Figure A.6: Air gap axial pressure loss.

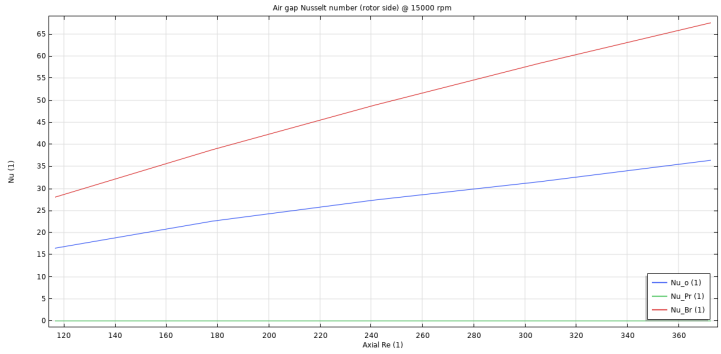

(a) Nu_R @ fixed mass flow rate (0 kg/s).

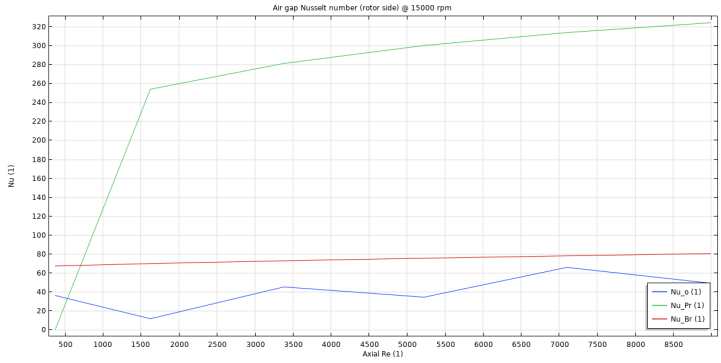

(b) Nu_R @ fixed rotational speed (15 000 rpm).

Figure A.7: Nusselt number (rotor side) coefficient comparison.

A.10 ACM m^*-Analysis

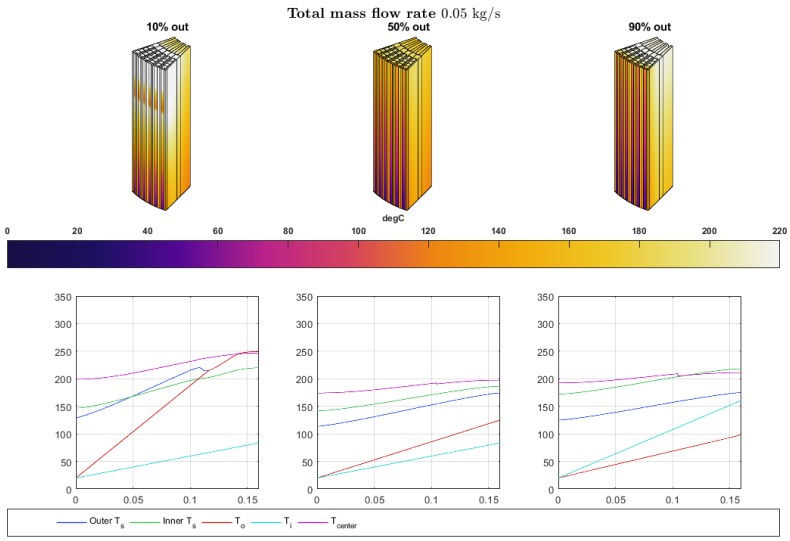

Figure A.8: Temperature distribution @ varying m^*, $\dot{m} = 0.05kg/s$.

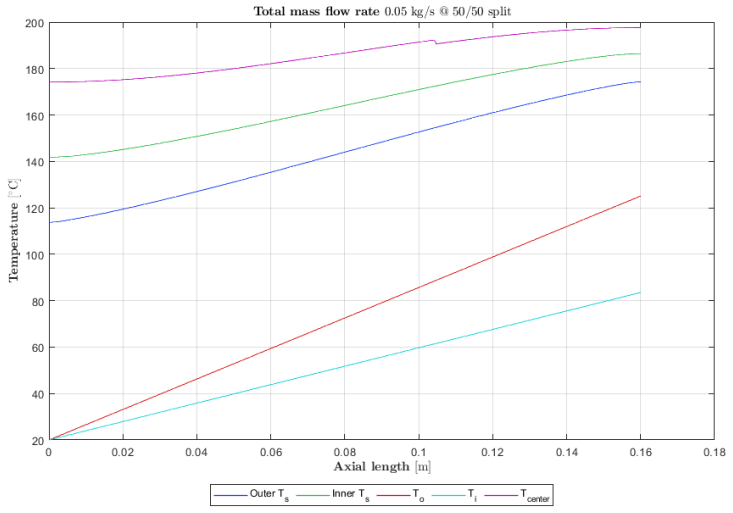

Figure A.9: Axial temperature evolution @ $m^* = 0.5$, $\dot{m} = 0.05kg/s$.

A.11 International Standard Atmosphere

The standard atmosphere as reported by the International Organization for Standardization, normalized for sea level conditions.

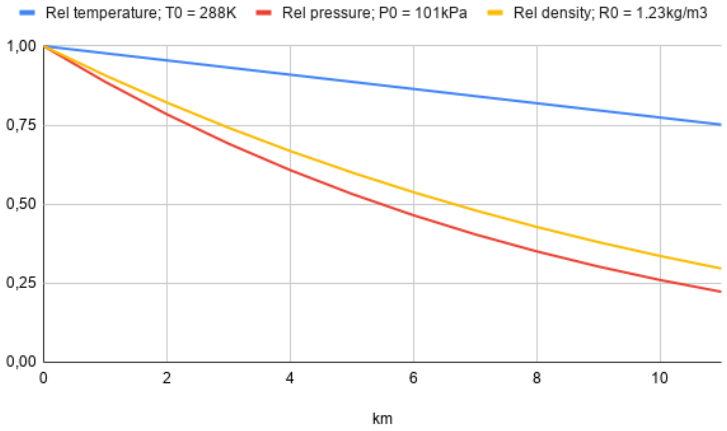

Figure A.10: International standard atmosphere.

A.12 Winding Equivalent Thermal Conductivity

All following equations have been modified to fit with the current nomenclature.

Staton, Boglietti, and Cavagnino 2003:

$$k_{W,\tau} = 0.1076 \cdot PF + 0.029967 \tag{A.14}$$

Hashin and Shtrikman 1962:

$$k_{W,\tau} = k_{nc} \frac{k_C \overline{PF} + k_{nc} \underline{PF}}{k_C \underline{PF} + k_{nc} \overline{PF}} \tag{A.15}$$

$$\overline{PF} = 1 + PF \tag{A.16}$$

$$\underline{PF} = 1 - PF \tag{A.17}$$

$$k_{nc} = k_E \tag{A.18}$$

Milton 1981:

$$k_{W,\tau} = k_{nc} \frac{(k_C \overline{PF} + k_{nc} \underline{PF})(k_C + k_{nc}) - \xi \underline{PF}(k_C - k_{nc})^2}{(k_C \underline{PF} + k_{nc} PF)(k_C + k_{nc}) - \xi \underline{PF}(k_C - k_{nc})^2} \tag{A.19}$$

$$\overline{PF} = 1 + PF \tag{A.20}$$

$$\underline{PF} = 1 - PF \tag{A.21}$$

$$k_{nc} = k_E \tag{A.22}$$

With ξ-values tabulated by Torquato and Lado 1988:

PF	0.1	0.2	0.3	0.4	0.5	0.6	0.65
ξ	0.032	0.063	0.092	0.12	0.17	0.25	0.37

Simpson, Wrobel, and Mellor 2013:

$$k_{W,\tau} = k_{nc}\frac{(1+v_C)k_C + (1-v_C)k_{nc}}{(1-v_C)k_C + (1+v_C)k_{nc}} \tag{A.23}$$

$$v_C = PF\left(\frac{R_C}{R_{ws}}\right)^2 \tag{A.24}$$

$$k_{nc} = k_E\frac{v_E}{v_E+v_I} + k_I\frac{v_I}{v_E+v_I} \tag{A.25}$$

$$v_E = 1 - PF \tag{A.26}$$

$$v_I = PF\left(\frac{2R_C t_I + t_I^2}{R_{ws}^2}\right) \tag{A.27}$$

Ayat et al. 2018:

$$k_{W,\tau} = \left[\frac{\ln\frac{R_C}{R_{ws}\sqrt{PF}}}{k_E} + \frac{\ln\frac{R_{ws}}{R_C}}{k_I} + \frac{1}{k_C}\right]^{-1} \tag{A.28}$$

Liu et al. 2019:

$$k_{W,\tau} = k_E\frac{k_{ws}\overline{PF} + k_E\underline{PF}}{k_{ws}\underline{PF} + k_E\overline{\overline{PF}}} \tag{A.29}$$

$$k_{ws} = k_I\frac{k_C(1+\chi) + k_I(1-\chi)}{k_C(1-\chi) + k_I(1+\chi)} \tag{A.30}$$

$$\chi = \left(\frac{R_C}{R_{ws}}\right)^2 \tag{A.31}$$

t

Jaritz and Biela 2013 (orthogonal):

$$\mathbb{R}_{th,\square} = \left[2k_E C_1 L_A \left(C_2 + \frac{k_E}{8k_I} \left(\frac{2t_I}{R_{ws}} \right)^2 C_3 C_1 \right) \right]^{-1} \tag{A.32}$$

$$\begin{aligned} k_{W,\tau} &= \frac{R_{ws}}{\mathbb{R}_{th,\square} R_C L_A} \\ &= \frac{2k_E C_1 R_{ws}}{R_C} \left[C_2 + \frac{k_E}{8k_I} \left(\frac{2t_I}{R_{ws}} \right)^2 C_3 C_1 \right] \end{aligned} \tag{A.33}$$

$$C_1 = \left[1 - \frac{k_E t_I}{k_I R_{ws}} \right]^{-1} \tag{A.34}$$

$$C_2 = \arctan\left(\sqrt{\frac{C_1 + 1}{C_1 - 1}} \right) \frac{C_1}{\sqrt{C_1^2 - 1}} - \frac{\pi}{4} \tag{A.35}$$

$$C_3 = \frac{C_1 (C_1^2 - 2)}{(C_1^2 - 1)^{3/2}} \arctan\left(\sqrt{\frac{C_1 + 1}{C_1 - 1}} \right) \frac{C_1}{2C_1^2 - 2} - \frac{\pi}{4} \tag{A.36}$$

$$PF = \frac{\pi R_C^2}{4R_{ws}^2} \quad , \quad \lim_{t_I \to 0} = \frac{\pi}{4} \approx 0.785 \tag{A.37}$$

Jaritz and Biela 2013 (orthocyclic):

$$\mathbb{R}_{th,\triangle} = \left[4k_E L_A \left(C_4 + C_5 \left(\frac{k_E t_I}{k_I R_{ws}^2}\right)\left(R_C + \frac{t_I}{2}\right)\right)\right]^{-1} \tag{A.38}$$

$$\begin{aligned} k_{W,\tau} &= \frac{\sqrt{3}R_{ws}}{2\mathbb{R}_{th,\triangle} R_C L_A} \\ &= \frac{2\sqrt{3}k_E R_{ws}}{R_C}\left[C_4 + C_5\left(\frac{k_E t_I}{k_I R_{ws}^2}\right)\left(R_C + \frac{t_I}{2}\right)\right] \end{aligned} \tag{A.39}$$

$$C_1' = 1 - \frac{k_E t_I}{k_I R_{ws}} \tag{A.40}$$

$$C_4 = \int_0^{\frac{\pi}{6}} \frac{\cos^2\theta - \cos\theta\sqrt{\cos^2\theta - 0.75} - 0.5}{\left[\cos\theta - C_1'(\sqrt{\cos^2\theta - 0.75} + 0.5)\right]^2} d\theta \tag{A.41}$$

$$C_5 = \int_0^{\frac{\pi}{6}} \frac{\sin^2\theta + \cos\theta\sqrt{\cos^2\theta - 0.75}}{\left[\cos\theta - C_1'(\sqrt{\cos^2\theta - 0.75} + 0.5)\right]^2} d\theta \tag{A.42}$$

$$PF = \frac{\pi R_C^2}{2\sqrt{3}R_{ws}^2} \quad , \quad \lim_{t_I \to 0} = \frac{\pi}{2\sqrt{3}} \approx 0.907 \tag{A.43}$$

Yi et al. 2019:

$$k_{lz} = \frac{H}{W(\Lambda \sec\phi - 2H \csc\phi)\mathbb{R}_{th,lz}} \tag{A.44}$$

$$\mathbb{R}_{th,lz} = 2\mathbb{R}_{lz,\tau}\frac{10\mathbb{R}_{lz,\tau}^2 + 11\mathbb{R}_{lz,\tau}\mathbb{R}_{lz,\lambda} + 2\mathbb{R}_{lz,\lambda}^2}{2\mathbb{R}_{lz,\tau}^2 + 8\mathbb{R}_{lz,\tau}\mathbb{R}_{lz,\lambda} + \mathbb{R}_{lz,\lambda}^2} \tag{A.45}$$

$$\mathbb{R}_{lz,\lambda} = \frac{2}{Wk_\lambda PF_{lz}}\frac{\Lambda \sec\phi - H(2-n)\csc\phi}{nH} \tag{A.46}$$

$$\mathbb{R}_{lz,\tau} = \frac{nk_E H}{k_\tau W(\Lambda \sec\phi - 2H \csc\phi)}\frac{k_\tau \overline{PF}_{lz} + k_E \underline{PF}_{lz}}{k_\tau \underline{PF}_{lz} + k_E \overline{PF}_{lz}} \tag{A.47}$$

$$\phi = \arctan\left(\frac{2(H+W)}{\Lambda}\right) \tag{A.48}$$

$$H = 4R_{ws} \tag{A.49}$$

$$W = 4nR_{ws} \tag{A.50}$$

$$\overline{PF}_{lz} = 1 + PF_{lz} \tag{A.51}$$

$$\underline{PF}_{lz} = 1 - PF_{lz} \tag{A.52}$$